NOTES AND CORRESPONDENCE

On Dipolelike Variability of Sea Surface Temperature in the Tropical Indian Ocean

ASTRID BAQUERO-BERNAL, MOJIB LATIF, AND STEPHANIE LEGUTKE

Max-Planck-Institut für Meteorologie, Hamburg, Germany

25 January 2001 and 29 November 2001

ABSTRACT

The interannual variability of the tropical Indian Ocean sea surface temperature (SST) is studied with observational data and a hierarchy of coupled general circulation models (CGCMs). Special attention is given to the question of whether an oscillatory dipole mode exists in the tropical Indian Ocean region with centers east and west of 80°E. These results indicate that dipolelike variability can be explained as an oscillatory mode only in the context of El Niño–Southern Oscillation (ENSO).

A dipolelike structure in the SST anomalies independent of ENSO was found also. This series of coupled model experiments shows that ocean dynamics is not necessary to this type of dipolelike SST variability. It is forced by surface heat flux anomalies that are integrated by the thermal inertia of the oceanic mixed layer, which reddens the SST spectrum.

1. Introduction

Since the interannual variability in the tropical Indian Ocean sea surface temperature (SST) is much weaker than that in the Pacific, it did not receive so much attention and is less well understood than the variability in the Pacific. The latter is dominated by the El Niño–Southern Oscillation (ENSO) phenomenon. Although ENSO originates in the tropical Pacific, it affects the global climate. Several investigations have suggested that ENSO also influences the Indian Ocean in different ways (Latif and Barnett 1995; Meyers 1996; Tourre and White 1997; Chambers et al. 1999; Venzke et al. 2000). Other studies have suggested that a significant fraction of the SST variability is related to ENSO but that there are other factors that are also important in determining the SST anomalies (SSTA; Reverdin et al. 1986; Murtugudde and Busalacchi 1999). Recently, Saji et al. (1999) and Webster et al. (1999) have proposed the existence of a coupled ocean–atmosphere mode that originates in the Indian Ocean climate system, which has characteristic seasonal phase locking and may induce anomalous rainfall over eastern Africa and Indonesia. Furthermore, it is argued that the mode is independent of ENSO. The mode is referred to as the ''dipole mode'' (DM). The DM spatial structure they proposed is characterized by SSTAs of one sign in the southeastern tropical Indian Ocean (SETIO; 10°S–0°, 90°–110°E) and SSTAs of the opposite sign in the western tropical Indian Ocean (WTIO; 10°S–10°N, 50°–70°E). However, the existence of a dipole as a mode of SST variability independent of ENSO is currently a subject of discussion. Allan et al. (2001) show evidence that supports the dependence, rather than independence, of ENSO and Indian Ocean dipole.

Here we investigate the interannual variability in the tropical Indian Ocean SST and its relationship to ENSO in more detail. SST observations and results from a series of coupled model integrations are used. We apply correlation analyses using area-averaged anomalies and the technique of principal oscillation patterns (POPs) to remove the ENSO signal. POP analysis is designed to extract the characteristic space–time variations within a complex multidimensional system (Hasselmann 1988; von Storch et al. 1988; Xu and von Storch 1990). We show that an oscillatory dipolelike structure like the one proposed by Saji et al. (1999) exists only as part of the ENSO cycle. There exists, however, dipolelike variability in the Indian Ocean independent of ENSO, but this type of variability is driven by the atmosphere.

The paper is organized as follows. The results of the analyses of the observed SSTs are presented in section 2. We describe the results of the coupled model simulations in section 3. We present our major conclusions in section 4.

Corresponding author address: Dr. Mojib Latif, Max-Planck-Institut für Meteorologie, Bundesstrasse 55, Hamburg D-20146, Germany.
E-mail: latif@dkrz.de

2. SST observations

We use the monthly SST dataset of the Hadley Centre for Climate Prediction and Research (Folland et al.

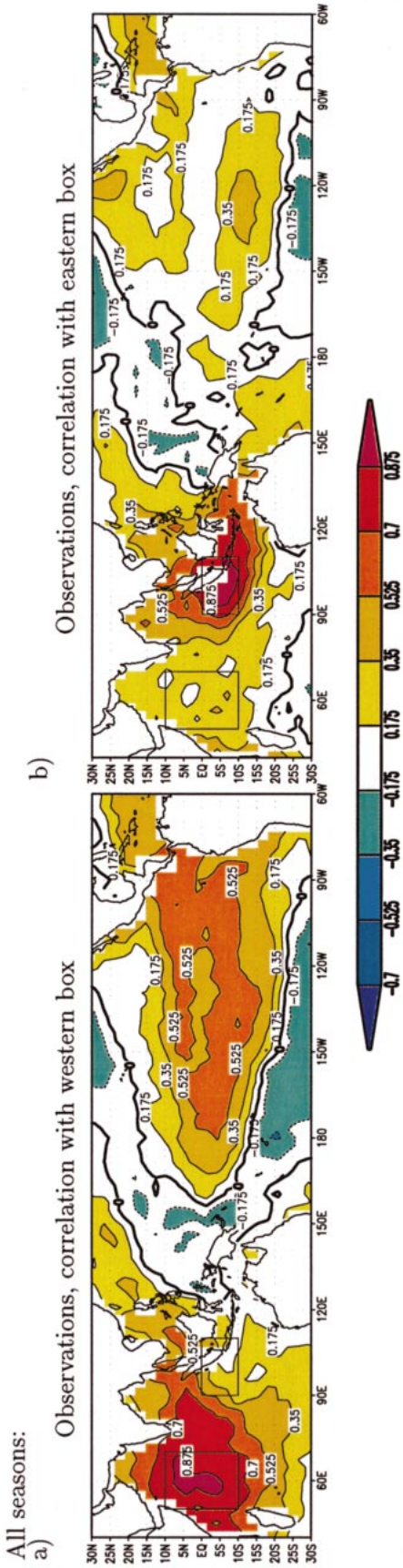

FIG. 1. Correlation of (a) WTIO box-averaged SSTAs, and (b) SETIO box-averaged SSTAs with Indo-Pacific SST anomalies for all seasons. SSTAs from the Hadley Centre observational dataset, 1949–98. Correlations exceeding (a) 0.31 and (b) 0.30 are significant at the 95% confidence level.

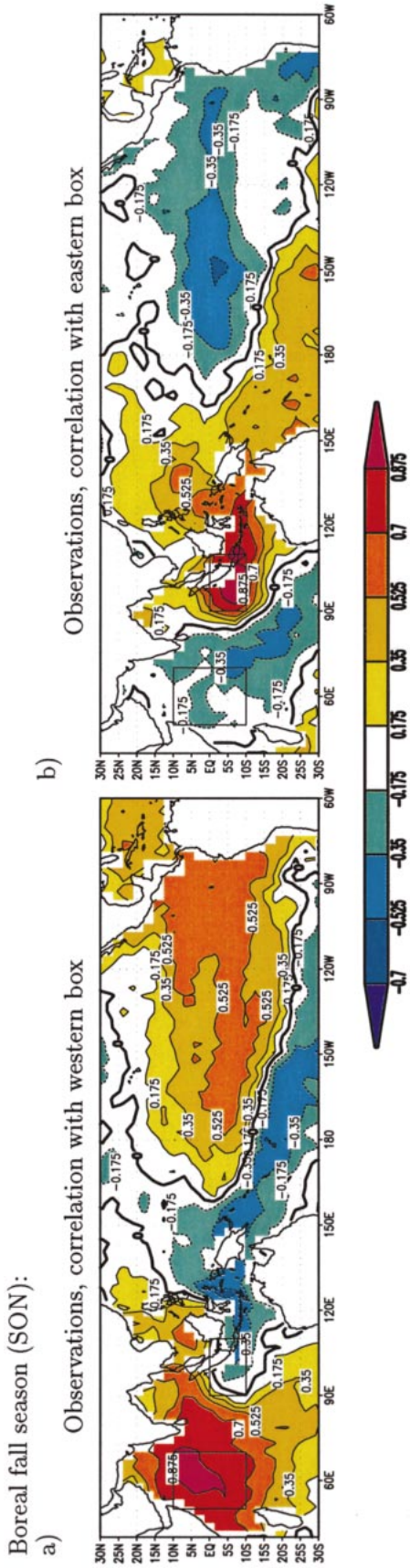

FIG. 2. Correlation of (a) WTIO box-averaged SSTAs, and (b) SETIO box-averaged SSTAs with Indo-Pacific SSTAs for SON. SSTAs from the Hadley Centre observational dataset, 1949–98. Correlations exceeding (a) and (b) 0.27 are significant at the 95% confidence level.

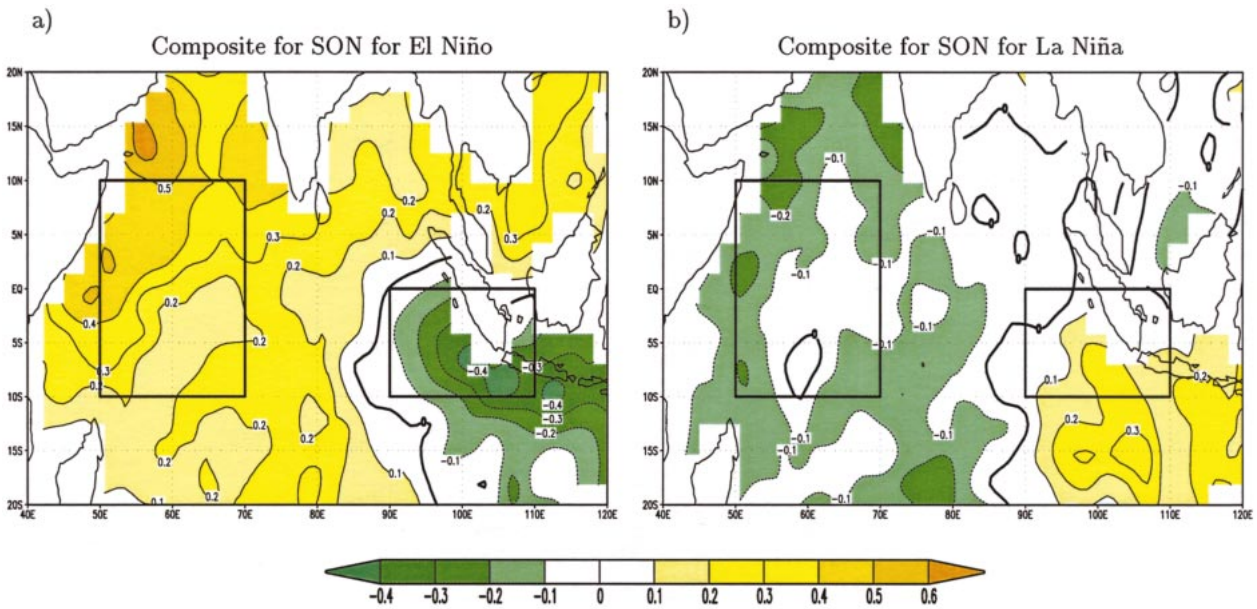

FIG. 3. Composites for SON for El Niño and La Niña events. (a) Composite of the SSTAs in SON for the six recent El Niño events. (b) Composite of the SSTAs in SON for the seven recent La Niña events. Units are given in °C.

1999). Although the dataset covers the period 1870–1998, we analyzed only the period 1949–98, which is commonly believed to be the most reliable period. The SSTAs were calculated by subtracting the mean annual cycle and the linear trend at each grid point. This procedure was used for the analyses of the observations and simulations. We consider the region 30°S–30°N and 40°E–60°W, which corresponds to the tropical Indian and Pacific Oceans. To perform the correlations between global and box-averaged SSTAs we always used mean seasonal values. For each correlation map we calculated the 95% significant level by applying a *t* test. The estimation of the number of degrees of freedom was performed based upon the approximation by Zwiers and von Storch 1995. We also performed a POP analysis based on monthly values in order to identify the ENSO-related SST variability and to remove it from the full observational dataset.

a. Analysis considering all the seasons

The correlations of the Indo-Pacific SSTAs with box-averaged SSTAs in SETIO and WTIO are shown in Fig. 1. The WTIO box shows significant correlations with equatorial SSTAs in the Pacific Ocean, but it has no negative correlation with the anomalies in SETIO (Fig. 1a). The SETIO box does not show either any significant positive or negative correlation with the SSTAs in WTIO, and the correlations with the SSTAs in the Pacific are smaller. Both correlation maps (Figs. 1a and 1b) lead to the conclusion that the SSTAs in SETIO and in WTIO are not significantly negatively correlated with each other at lag zero, which is consistent with the results of Dommenget and Latif (2002). Additionally, we performed lagged cross-correlation analyses between the SSTAs in SETIO and those in WTIO. We found that maximum cross correlation ($r = 0.43$) occurs when the SST variations in SETIO lag those in WTIO by one season. Higher correlations are found when the cross-correlation analysis is performed with respect to the Niño-3 time series. We found maximum cross correlation ($r = 0.65$) when the SSTAs in the western Indian Ocean lag those of the eastern Pacific by about one season, which is consistent with the results of Venzke et al. (2000). Maximum cross correlation ($r = 0.48$) is obtained when the SSTAs in the eastern Indian Ocean lag those of the eastern Pacific by two seasons. This lag of two seasons is consistent with the fact that the SSTAs in SETIO lag those in WTIO by one season. At lag zero, the correlation between WTIO and Niño-3 time series amounts to 0.6. It should be noted that the correlation between the SSTAs in SETIO and Niño-3 at lag zero is also positive.

In summary, the results of the correlation analyses and the cross-correlation analyses with respect to the SSTA in the eastern Pacific (Niño-3) reveal that the SST variability in the Indian Ocean is strongly remotely forced by the ENSO phenomenon. Furthermore, a dipolelike pattern cannot be identified if all seasons are considered.

b. Seasonal analyses

In the next step, we computed the correlation maps for every season separately (like those shown in Fig. 1). No negative correlation was found between the SSTAs in SETIO and WTIO neither in winter nor in spring (not shown). For the boreal summer season, there

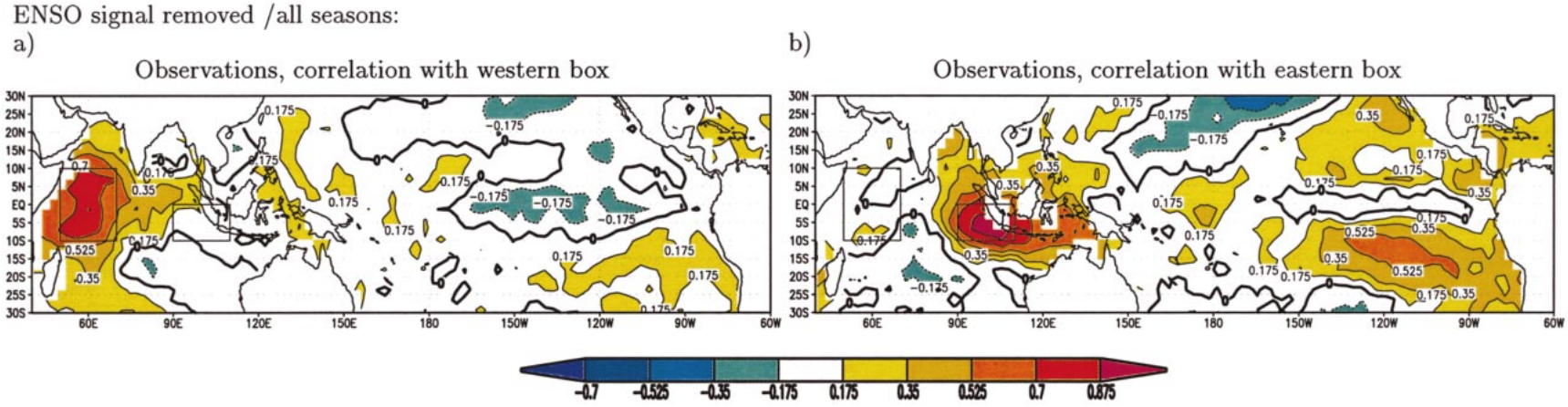

FIG. 4. Correlation of (a) WTIO box-averaged SSTAs, and (b) SETIO box-averaged SSTAs with Indo-Pacific SSTAs for all seasons. SSTAs from the Hadley Centre observational dataset, 1949–98. The ENSO signal was subtracted prior to the analysis. Correlations exceding (a) 0.21 and (b) 0.30 are significant at the 95% confidence level.

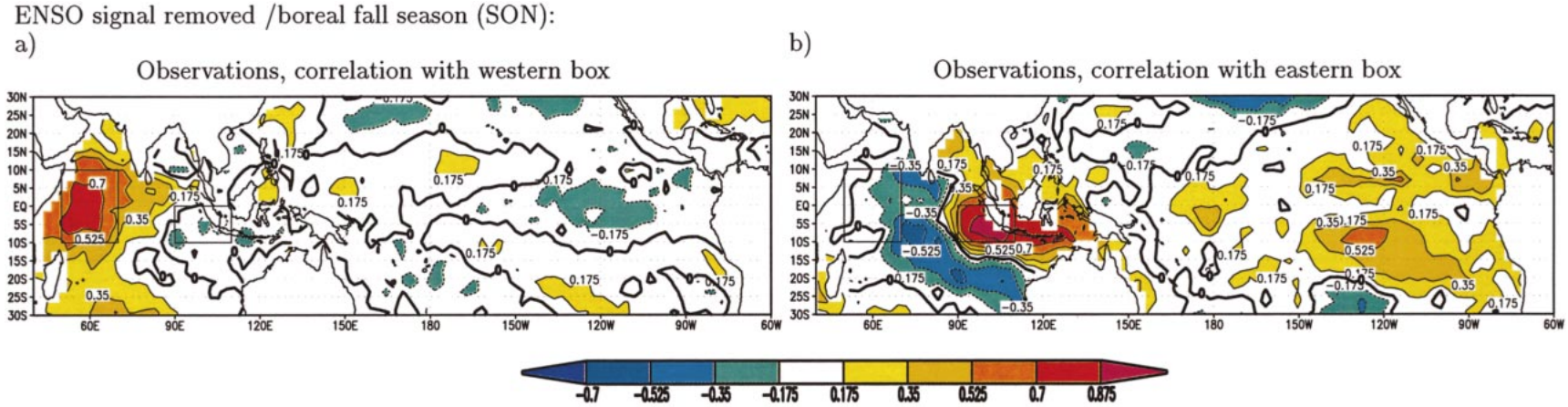

FIG. 5. Correlation of (a) WTIO box-averaged SSTAs, and (b) SETIO box-averaged SSTAs with Indo-Pacific SSTAs for SON. SSTAs from the Hadley Centre observational dataset, 1949–98. The ENSO signal was subtracted prior to the analysis. Correlations exceding (a) 0.32 and (b) 0.27 are significant at the 95% confidence level.

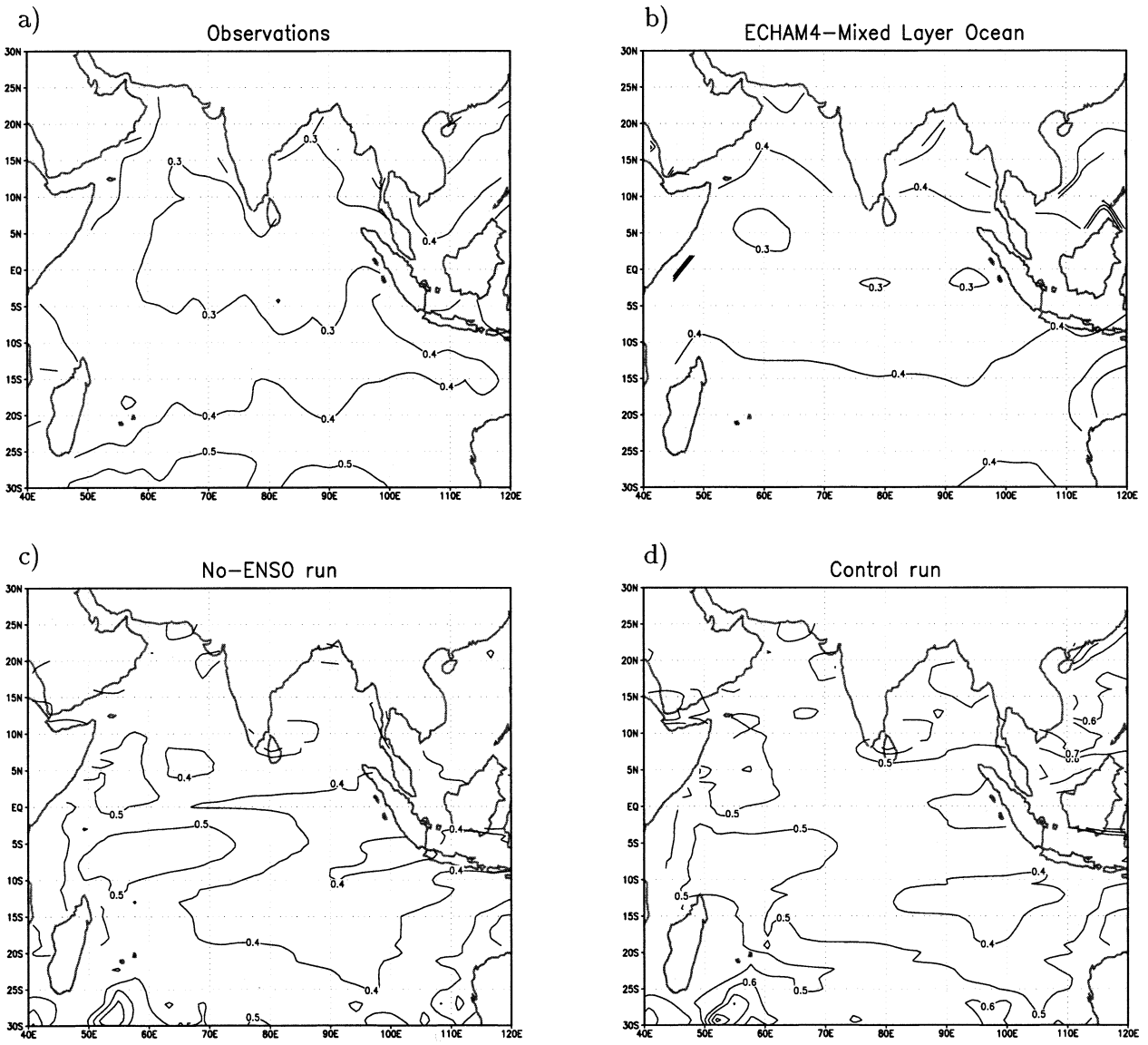

FIG. 6. Spatial distribution of the std dev of the SSTAs. (a) For the Hadley Centre observational dataset, (b) for the ECHAM4/mixed layer ocean simulation, (c) for the no-ENSO run of the CGCM ECHO-G, and (d) for the control run. Units are given in °C.

is a very weak negative correlation between the SSTAs in the WTIO and those near the western coast of Indonesia and the northwestern coast of Australia (not shown). Some stronger cross–Indian Ocean gradient, however, was found in boreal fall. More importantly, this is the season when a strong correlation between the surface westerlies over the equatorial Indian Ocean and the rainfall at the coast of East Africa can be found (Hastenrath et al. 1993). Accordingly, the boreal fall season [September–October–November (SON)] will be considered in detail.

c. Analysis for SON

We turn now to the boreal fall season. The SSTAs in WTIO show negative correlations with those in the eastern Indian Ocean, but they are restricted to a small region (Fig. 2a). The SETIO SSTAs do show negative correlations with those in the central Indian region, which are strongest south of the equator (Fig. 2b). Both correlation maps, however, show that the SSTAs in SETIO and in WTIO are not strongly negatively correlated with each other. Furthermore, the SSTAs in the two boxes, SETIO and WTIO, are significantly correlated with the SSTAs in the Pacific.

Figure 3 shows the composites for El Niño and La Niña events. Figure 3a shows the composite for the six recent El Niño events (1957, 1965, 1972, 1982, 1987, and 1997) and Fig. 3b that for the seven recent La Niña events (1955, 1970, 1971, 1973, 1975, 1985, and 1988). ENSO-related variability in the Indian Ocean in the bo-

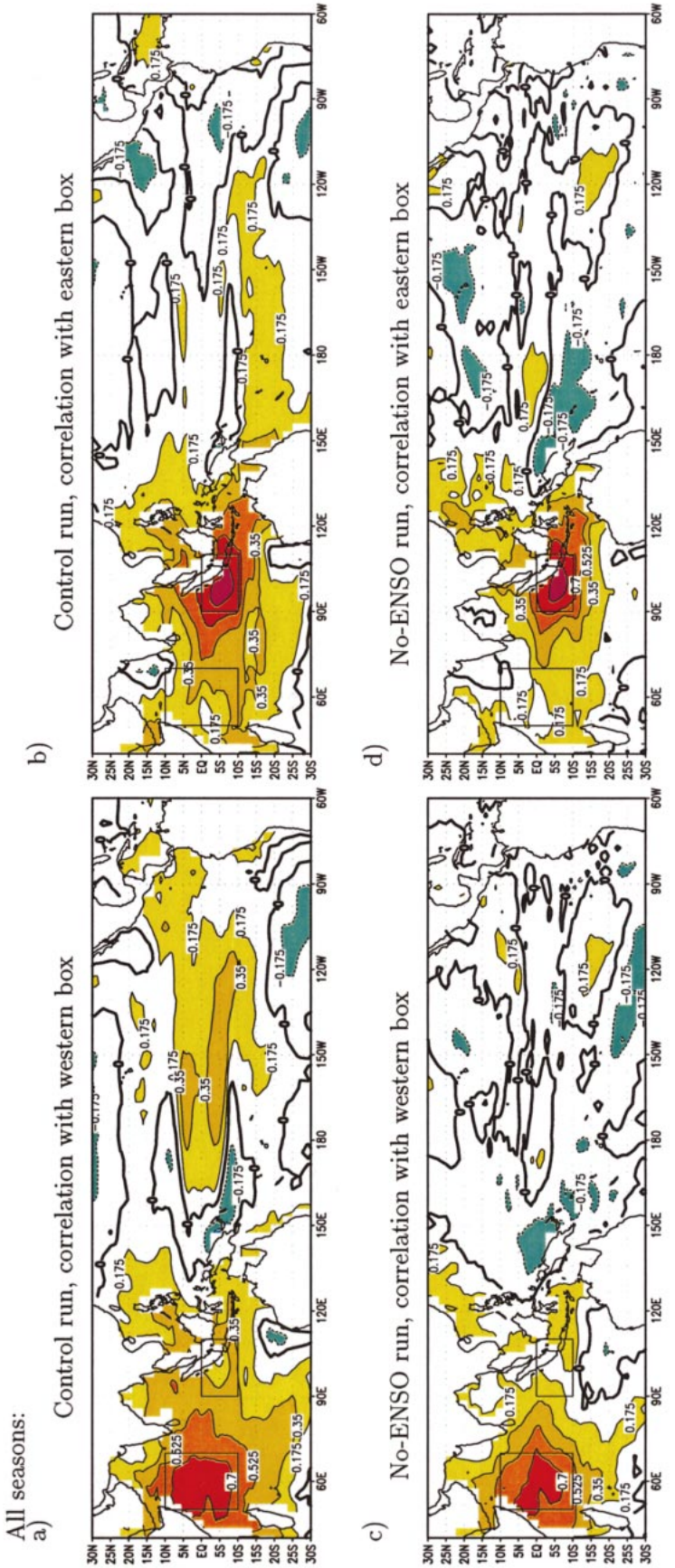

FIG. 7. Correlation of WTIO box-averaged SSTAs, SETIO box-averaged SSTAs with Indo-Pacific SSTAs for all seasons. (a) and (b) SSTAs from the control run of the CGCM ECHO-G. (c) and (d) SSTAs from the no-ENSO run. In (a) and (c) correlations are with respect to the WTIO. In (b) and (d) correlations are with respect to SETIO. Correlations exceeding (a) 0.15 (b) 0.16, (c) 0.12, (d) 0.13 are significant at the 95% confidence level.

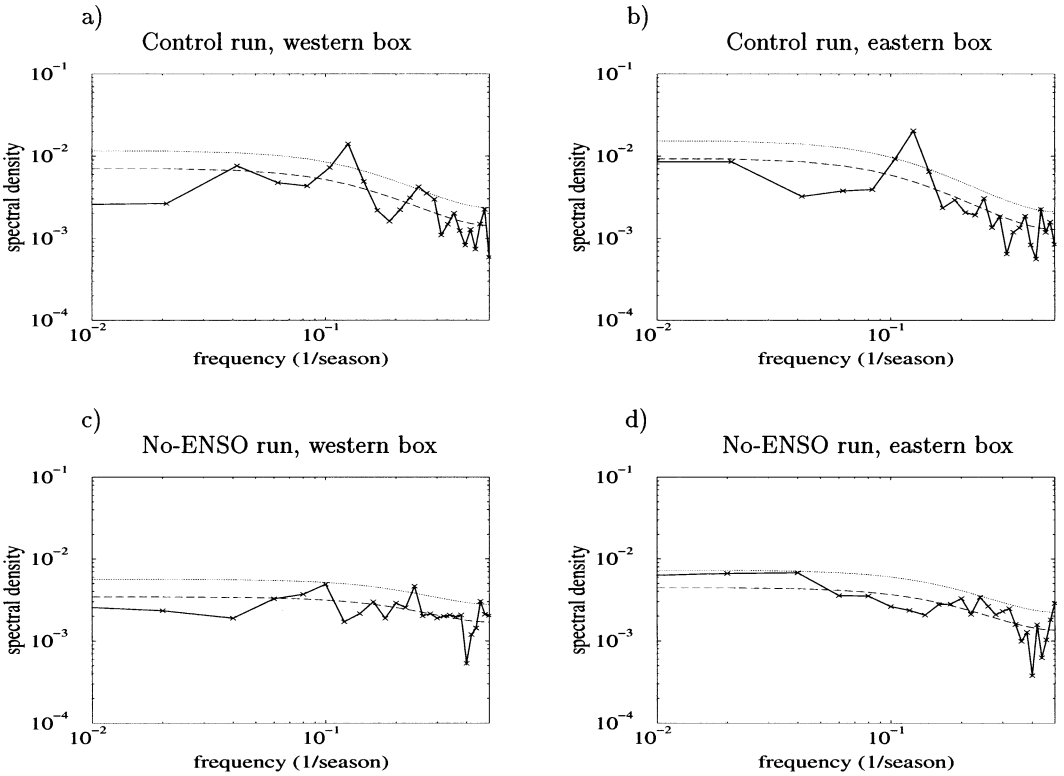

FIG. 8. Spectra of box-averaged SSTAs in the SETIO and WTIO regions when all the seasons are considered. (a) and (b) SSTAs from the control run with the CGCM ECHO-G. (c) and (d) SSTAs from the no-ENSO run. In (a) and (c) spectra are for WTIO. In (b) and (d) spectra are for SETIO. The thin solid lines are the expected red noise spectra. The dashed lines are the 95% confidence level for the null hypothesis of a red noise spectra.

real fall season looks like a seesaw: for the El Niño events, there are positive SST anomalies west of 80°E and negative anomalies east of 80°E. The situation is reversed during La Niña conditions, but the magnitude of the anomalies is smaller in the western region. Figures 2 and 3 demonstrate clearly that the dipolelike variability in the tropical Indian Ocean is not independent of the ENSO phenomenon.

d. ENSO-removed analyses

Our analyses may be influenced by the presence of the strong ENSO signal. We therefore repeated the correlation analyses by removing the ENSO signal prior to the analyses. There is no unique way to do this. Here we subtracted the leading POP mode from the monthly SSTA. Seasonal mean values were then computed from the residual dataset.

The POP analysis of the monthly SSTAs revealed 1 dominant POP pair (the ENSO mode, not shown) accounting for 26.4% of the total variance. The rotation period of this POP pair amounts to 42 months, with a decay time of 10 months. All other POPs were statistically insignificant. The dominant POP pair is clearly associated with ENSO, which can be inferred from the correlation of the complex coefficient time series (not shown) with the Niño-3 (5°S–5N, 150°–90°W) SSTA time series. The zero lag correlation of the real part time series with the Niño-3 time series amounts to 0.94 and the 4-month lag correlation of the imaginary part time series with the Niño-3 time series amounts to 0.74. A cross-spectral analysis of the two coefficient time series (not shown) showed the theoretically expected result that they are highly coherent (above the 99% significance level) with a phase shift of about $-90°$ for periods between 20 and 70 months.

1) ANALYSIS CONSIDERING ALL THE SEASONS

The correlations of the Indo-Pacific SSTAs with the averaged SSTAs in SETIO and WTIO based on seasonal values are shown in Fig. 4. Again (as shown in Fig. 1 by retaining the full dataset), the correlation maps obtained from the ''ENSO-removed'' data show that the SSTA in the eastern and western parts of the Indian Ocean are not significantly correlated with each other, when we consider all four seasons together.

2) ANALYSIS FOR SON

Figure 5 shows the correlations of the Indo-Pacific SSTAs with box-averaged SSTAs in SETIO and WTIO

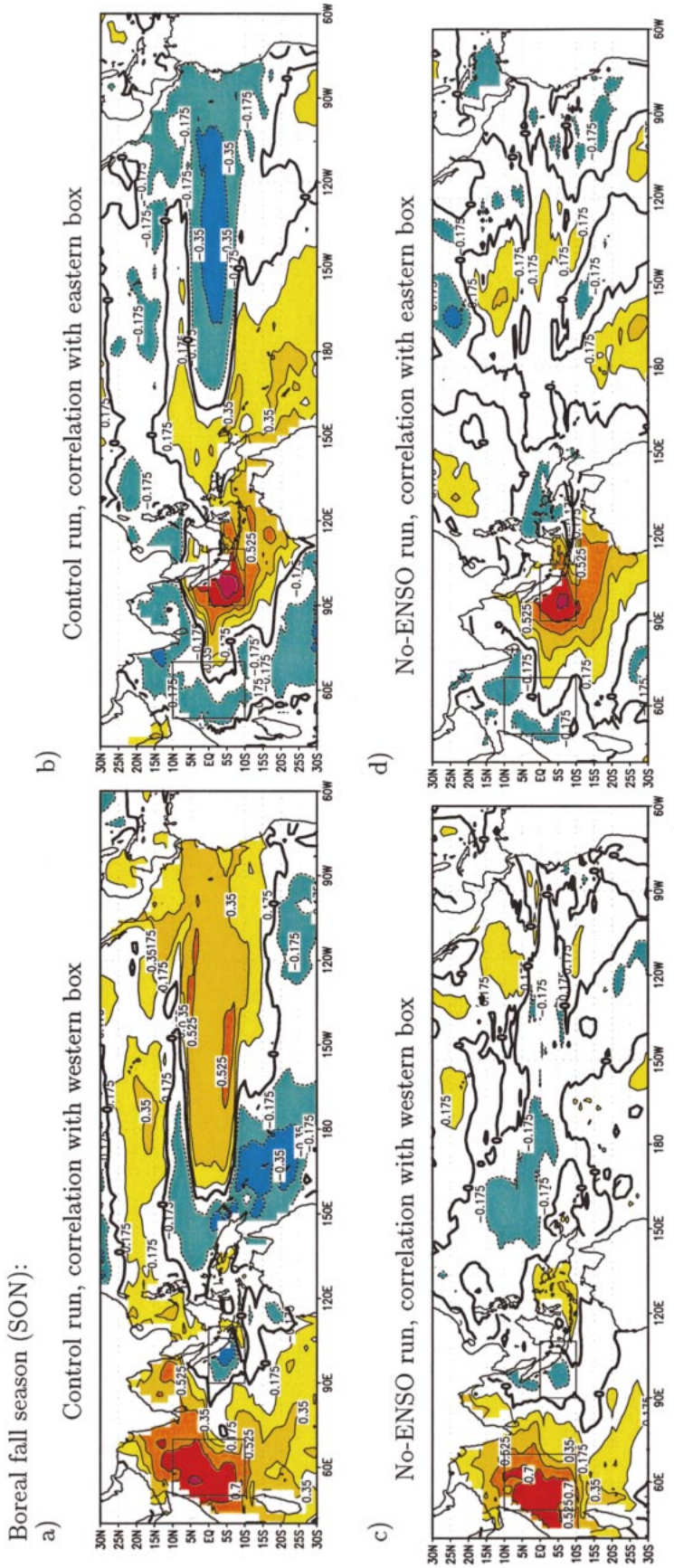

FIG. 9. Correlation of WTIO box-averaged SSTAs, SETIO box-averaged SSTAs, with Indo-Pacific SSTAs for SON. (a) and (b) SSTAs from the control run of the CGCM ECHO-G. (c) and (d) SSTAs from the no-ENSO run. In (a) and (c) correlations are with respect to the WTIO. In (b) and (d) correlations are with respect to SETIO. Correlations exceeding (a), (b), (d) 0.20 and (c) 0.24 are significant at the 95% confidence level.

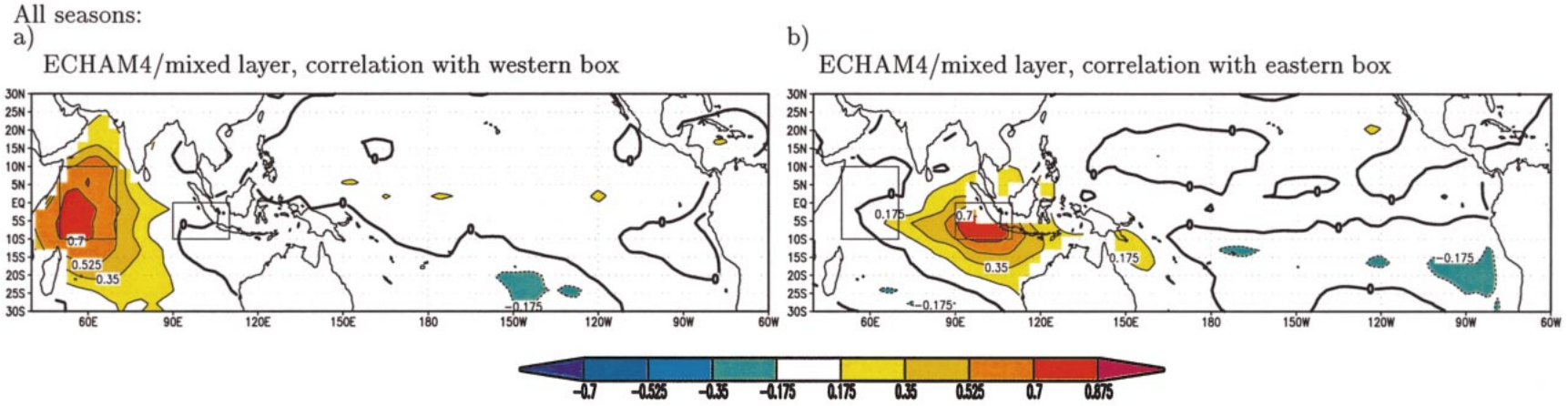

FIG. 10. Correlation of (a) WTIO box-averaged SSTAs, and (b) SETIO box-averaged SSTAs with Indo-Pacific SSTAs for all seasons. The SSTAs are from the ECHAM4/mixed layer ocean simulation. Correlations exceding (a) 0.16 and (b) 0.20 are significant at the 95% confidence level.

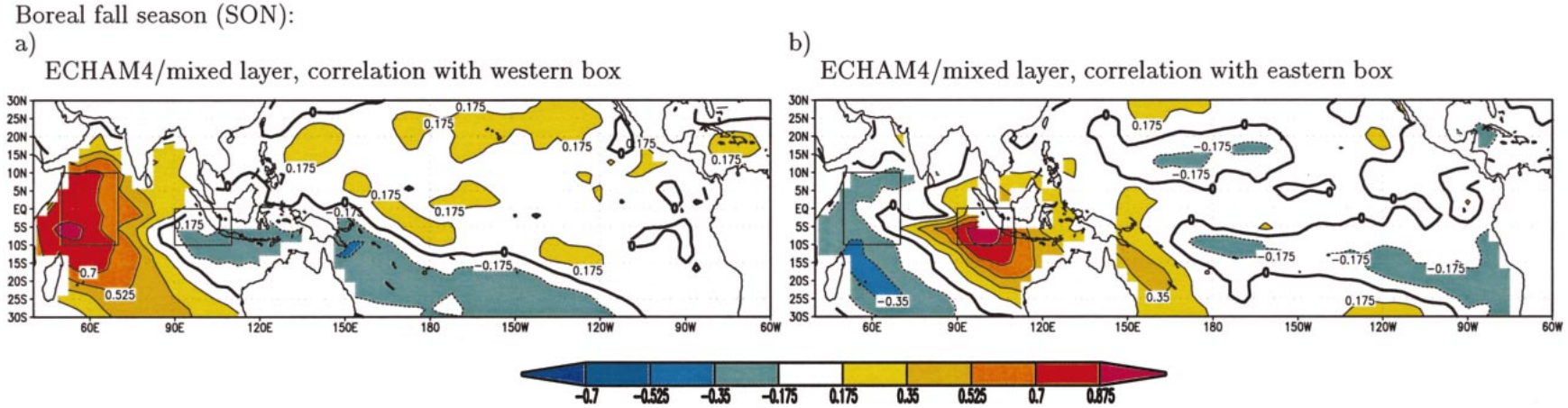

FIG. 11. Correlation of (a) WTIO box-averaged SSTAs, and (b) SETIO box-averaged SSTAs with Indo-Pacific SSTAs for SON. SSTAs are from the ECHAM4/mixed layer ocean simulation. Correlations exceding (a) 0.20 and (b) 0.22 are significant at the 95% confidence level.

for the fall season. A negative correlation between the SSTAs in SETIO and those in the central (but not western) Indian Ocean is seen in Fig. 5b. These negative correlations are larger than those in Fig. 2b and they extend to the north of the equator. In conclusion, Figs. 2, 4, and 5 show that SSTAs in the eastern and western parts of the Indian Ocean are not strongly negatively correlated, and that there is a significant negative correlation between the SSTAs in the eastern and central parts of the Indian Ocean during the boreal fall season. This negative correlation between the eastern and central regions exists also when the ENSO signal is removed from the data. In the next section we shall discuss the mechanisms that may explain this dipolelike variability by analyzing a suite of coupled model simulations.

3. Coupled model simulations

We turn now to the coupled model simulations. We analyzed three different coupled model runs. The first coupled run is an extended range integration with the coupled ocean–atmosphere general circulation model (GCM) ECHO-G (Legutke and Voss 1999). This run serves as a control integration. The second coupled run is a similar run, but with the ENSO variability suppressed. The ocean GCM is replaced by a fixed-depth mixed layer model in the third coupled run. This set of coupled experiments enables us to investigate the roles of ENSO and ocean dynamics in the generation of the interannual SST variability of the tropical Indian Ocean. The ECHO-G model has a horizontal resolution of 2.8° × 2.8°. The ocean component uses a higher meridional resolution of 0.5° within the region 10°N–10°S. Here we use the first 100 years from the control run. The coupled run in which the ENSO variability has been suppressed (no-ENSO run) has also a duration of 100 years. The suppression of ENSO variability was realized in the coupled model by replacing the actual SSTs simulated by the ocean component in the tropical Pacific by climatology before passing them to the atmosphere model. We also used a mixed layer ocean model with the ECHAM4 atmosphere model (Roeckner et al. 1996, the same atmosphere model that has been used in the coupled runs discussed above). The mixed layer model has a constant depth of 50 m and does not carry by definition any ocean dynamics. Variations in the surface heat flux is the only mechanism that can produce SST anomalies in such a model. A sequence of 100 model years was available for analysis in this study.

The standard deviations of the SST anomalies for the observations and for the three coupled model simulations are shown in Fig. 6. The observations (Fig. 6a) exhibit a north–south gradient in the values of the standard deviation, with the largest values near 30°S. The variability in the mixed layer run (Fig. 6b) compares well to observations (Fig. 6a). The no-ENSO and control simulations (Figs. 6c and 6d) display somewhat larger variabilities. Compared with the control run, the no-ENSO run shows a reduction of about 0.1° in the SST variability almost everywhere in the tropical Indian Ocean Basin. For the tropical Pacific Ocean, the variability in the control run is about 10 times larger than the variability in the no-ENSO run (not shown). We also calculated the standard deviation maps for the boreal fall season separately (not shown). They exhibit similar patterns to those shown in Fig. 6: the SST variability increases with the complexity of the ocean model and a large part of the SST variability can be already produced in the mixed layer simulation, where the forcing mechanism is only due to surface heat flux anomalies.

a. Fully coupled ocean–atmosphere GCM

To examine the interannual variability independent of ENSO, the subtraction of the leading POP pair may not be the best method. We therefore analyzed additionally the outputs of the two simulations with the ECHO-G model. Figure 7 shows the SSTA-correlation maps with the box-averaged SST anomalies in the SETIO and WTIO regions when all seasons are considered. Both simulations, the control run (Figs. 7a and 7b) and the no-ENSO run (Figs. 7c and 7d), show positive correlations almost everywhere in the Indian Ocean. In particular, as in the observations, there is no negative correlation simulated in the two coupled runs between the western and eastern Indian Ocean. These model results confirm our observational results. We conclude further that our results do not depend on the way of subtracting the ENSO signal.

Figure 8 shows the spectra of box-averaged SST anomalies in the SETIO and WTIO regions for the control and no-ENSO runs. Each spectrum is tested against the hypothesis that the spectrum is produced by a first-order autoregressive process (red noise spectrum) and a 95% confidence level for accepting the red noise hypothesis is also shown. For the control run, the spectra of the two boxes (Figs. 8a and 8b) show enhanced variability for periods of 5–10 seasons, that is, about 1–3 yr (the coupled model simulates a quasi-biennial ENSO period). In contrast, the spectra of the no-ENSO run (Figs. 8c and 8d) are consistent with red noise spectra. This result indicates also that a dipole mode independent of ENSO that is associated with a specific timescale does not exist.

The correlation maps for fall (SON) are shown in Fig. 9. Both the control run and the no-ENSO run yield similar correlation maps. Although the correlations between the box-averaged SSTAs in SETIO and WTIO and the SSTAs in the Indian Ocean are low, there is some indication of dipolelike variability. This means that although ENSO was removed physically in the no-ENSO run, there is still a mechanism that produces a dipolelike structure in the SST anomalies in the boreal fall season. The correlation maps for the other seasons (not shown) do not exhibit a dipolelike structure.

b. AGCM coupled to a mixed layer ocean

Is the dipolelike variability in the no-ENSO run a result of ocean dynamics or of atmospheric forcing? In order

to answer this question, we performed correlation analyses for the SST anomalies from the mixed layer run.

Correlation analyses of SST anomalies from the mixed layer simulation are shown in Figs. 10 and 11. Figure 10 corresponds to the case when all the seasons are considered and Fig. 11 when only fall (SON) is considered. Both Figs. 10 and 11 show some correspondence with the maps derived from the observations (Figs. 1 and 2), and with those for the coupled runs (Figs. 7 and 9). The spectra of the SST anomalies in the boxes SETIO and WTIO considering all the seasons are consistent with the red noise assumption (not shown). It can be concluded from the results of the mixed layer simulation that an ENSO-independent dipolelike SST anomaly pattern exists in the boreal fall season, which can be explained by atmospheric forcing.

Dynamical processes in the ocean are not necessary to produce this type of bipolar SST variability. However, dynamical processes in the ocean and coupled ocean–atmosphere interactions may modify this type of variability.

4. Conclusions

Correlation analyses of seasonal SST anomalies from the Hadley Centre SST observations during the period 1949–98 and from three different coupled GCM runs show consistent results. The dominant SST variability in the tropical Indian Ocean is related to ENSO. The ENSO-related SST response of the Indian Ocean in the fall season is a dipole. However, we do not find evidence for an ENSO-independent oscillatory mode with dipolelike SST anomalies. Yet, dipolelike variability exists in the tropical Indian Ocean, but this type of variability is driven by the atmosphere and does not necessarily involve ocean dynamics.

Most studies so far described the ENSO response in the Indian Ocean as a homogeneous response: during El Niño events, the Indian Ocean exhibits basinwide warm SST anomalies and during La Niña conditions, the SST anomalies are of opposite sign. This is true for some seasons, especially for the winter season (DJF), but for fall (SON), this is generally not the case. We found that in the boreal fall season, on average, the ENSO signal can be seen as a dipolelike pattern: during El Niño events, cold anomalies are observed east of 80°E and warm SST anomalies west of 80°E, during La Niña events, we observe the reverse SST anomaly pattern.

An oscillatory ENSO-independent dipole mode does not exist in the tropical Indian Ocean. This has been validated by simulations with a hierarchy of coupled models. The only modelike dipole variability (in the physical sense that air–sea interactions lead to an oscillation) is associated with the ENSO phenomenon.

In summary, there is dipolelike variability in the SST of the Indian Ocean. This variability, however, is primarily associated with the ENSO phenomenon, but may also be forced stochastically by the atmosphere.

Acknowledgments. We would like to thank Dr. D. Dommenget for helpful discussions and suggestions. A. Baquero-Bernal is supported by the ''Francisco José de Caldas Institute for the Development of Science and Technology (COLCIENCIAS),'' under its scholarships program. Support is also given by the European Union's PROMISE project and by the German government through its Ocean CLIVAR project.

REFERENCES

Allan, R., and Coauthors, 2001: Is there an Indian Ocean dipole, and is it independent of the El Niño–Southern Oscillation? *CLIVAR Exch.,* **6** (3), 18–22.

Chambers, D. P., B. D. Tapley, and R. H. Stewart, 1999: Anomalous warming in the Indian Ocean coincident with El Niño. *J. Geophys. Res.,* **104** (C2), 3035–3047.

Dommenget, D., and M. Latif, 2002: A cautionary note on the interpretation of EOFs. *J. Climate,* **15,** 216–225.

Folland, C. K., D. Parker, A. Colman, and R. Washington, 1999: Large scale modes of ocean surface temperature since the late nineteenth century. *Beyond El Niño: Decadal and Interdecadal Climate Variability,* A. Navarra, Ed., Springer-Verlag, 73–102.

Hasselmann, K., 1988: PIPs and POPs: The reduction of complex dynamical systems using principal interaction and oscillation patterns. *J. Geophys. Res.,* **93,** 11 015–11 021.

Hastenrath, S., A. Nicklis, and L. Greischar, 1993: Atmospheric–hydrospheric mechanisms of climate anomalies in the western equatorial Indian Ocean. *J. Geophys. Res.,* **98** (C11), 20 219–20 235.

Latif, M., and T. P. Barnett, 1995: Interactions of the tropical oceans. *J. Climate,* **8,** 952–964.

Legutke, S., and R. Voss, 1999: The Hamburg atmosphere–ocean coupled circulation model ECHO-G. German Climate Computer Center (DKRZ) Tech. Rep. 18, 61 pp.

Meyers, G., 1996: Variation of Indonesian throughflow and El Niño–Southern Oscillation. *J. Geophys. Res.,* **101** (C5), 12 255–12 263.

Murtugudde, R., and A. Busalacchi, 1999: Interannual variability of the dynamics and thermodynamics of the tropical Indian Ocean. *J. Climate,* **12,** 2300–2326.

Reverdin, G., D. Cadet, and D. Gutzler, 1986: Interannual displacements of convection and surface circulation over the equatorial Indian Ocean. *Quart. J. Roy. Meteor. Soc.,* **112,** 43–67.

Roeckner, E., and Coauthors, 1996: The atmospheric general circulation model ECHAM4: Model description and simulation of present-day climate. Max-Planck-Institut für Meteorologie Rep. 218, Hamburg, Germany, 90 pp.

Saji, N. H., B. N. Goswami, P. N. Vinayachandran, and T. Yamagata, 1999: A dipole mode in the Indian Ocean. *Nature,* **401,** 360–363.

Tourre, Y. M., and W. B. White, 1997: Evolution of ENSO signals over the Indo-Pacific domain. *J. Phys. Oceanogr.,* **27,** 683–696.

Venzke, S., M. Latif, and A. Villwock, 2000: The coupled GCM ECHO-2. Part II: Indian Ocean response to ENSO. *J. Climate,* **13,** 1371–1383.

von Storch, H., T. Bruns, I. Fischer-Bruns, and K. Hasselmann, 1988: Principal Oscillation Pattern analysis of the 30–60 day oscillation in a GCM equatorial troposphere. *J. Geophys. Res.,* **93,** 11 022–11 036.

Webster, P. J., A. M. Moore, J. P. Loschnigg, and R. R. Leben, 1999: Coupled ocean–atmosphere dynamics in the Indian Ocean during 1997–1998. *Nature,* **401,** 356–360.

Xu, J. S., and H. von Storch, 1990: Principal Oscillation Pattern—Prediction of the state of ENSO. *J. Climate,* **3,** 1316–1329.

Zwiers, F. W., and H. von Storch, 1995: Taking serial correlation into account in tests of the mean. *J. Climate,* **8,** 336–351.